ELSEVIER

Polymer 44 (2003) 969–980

polymer

www.elsevier.com/locate/polymer

Catalyst impregnation and ethylene polymerization with mesoporous particle supported nickel-diimine catalyst

Zhibin Ye[a], Hatem Alsyouri[b], Shiping Zhu[a,*], Y.S. Lin[b]

[a]*Department of Chemical Engineering, McMaster University, 1280 Main Str., West, Hamilton, Ont., Canada L8S 4L7*
[b]*Department of Chemical Engineering, University of Cincinnati, Cincinnati, OH 45221, USA*

Received 24 April 2002; received in revised form 18 October 2002; accepted 18 November 2002

Abstract

A nickel-diimine catalyst (1,4-bis(2,6-diisopropylphenyl) acenaphthene diimine nickel(II) dibromide, DMN) was supported on mesoporous particles having parallel hexagonal nanotube pore structure (MCM-41 and MSF) for ethylene polymerization. The effects of supporting methods and particle morphological parameters, such as pore size and length, on the catalyst impregnation were systematically investigated. Pretreating the supports with methylaluminoxane (MAO) followed by DMN impregnation gave much higher catalyst loading and higher catalytic activity than the direct impregnation of DMN. The particle structure significantly affected the catalyst impregnation and this effect was explained with a semi-quantitative molecular diffusion model. Compared to homogeneous catalysts, significant reduction in activity was observed with the supported systems in ethylene polymerization. Extraction of active sites from the supports during polymerization was observed. The mesoporous supports exerted steric effects on unleached active sites, lowering chain walking ability, and producing polymers having lower short chain branch density. Replication of the particle morphology was observed in some polymer samples.

Keywords: Ethylene polymerization; Nickel-dimine catalyst; Mesoporous particle support

1. Introduction

Metallocene catalysts have a tremendous impact on polyolefin industries. Compared to classical multi-sited Ziegler–Natta catalysts, these single-site type catalysts offer unprecedented control over polymer chain structure and materials properties [1]. In addition to metallocene catalysts, a recent milestone in the area of organometallic catalyzed olefin polymerization is the discovery of the α-diimine derived late transitional metal (Ni or Pd) catalysts by Brookhart and co-workers [2–5]. Different from metallocenes, these catalysts can produce polyethylene with branch structures without comonomer incorporation due to a chain walking mechanism [2–10]. Control over the catalyst structures (diimine ligand and metal center), cocatalyst, and polymerization conditions (ethylene pressure, reaction temperature, etc) allows one to readily produce polyethylene grades from highly branched, completely amorphous materials to linear, semicrystalline, high-density materials by adjusting the competition between chain walking and chain propagation processes [2–12].

Supported metallocene catalysts have been widely investigated in industry and academia owing to the advantages in control of polymer particle morphology and applicability in gas-phase reactor technologies [13–16]. The most commonly used supports are spherical amorphous silica, alumina, and $MgCl_2$. Recently, new types of silicate and/or aluminosilicate-based mesoporous particles, i.e. MCM-41 and MSF (mesoporous silica fiber) [17–21], have been applied as support for metallocene and other catalysts for olefin polymerization [13–16,22–32]. The geometrical constraints of the nanotube pore structure of these particles as polymerization reactors affect the pattern of monomer insertion and chain growth processes, and thus offer a possible new route to control polymer chain structure and crystal morphology in olefin polymerization [22–32]. The work by Aida et al. [29] on the synthesis of fully extended chain crystal (ECC) polyethylene nanofibers with MSF-supported Cp_2TiCl_2 catalysts, termed as extrusion ethylene polymerization, demonstrated the good potential of

* Corresponding author. Tel.: +1-905-525-9140x24962; fax: +1-905-521-1350.
E-mail address: zhuship@mcmaster.ca (S. Zhu).

0032-3861/03/$ - see front matter © 2002 Elsevier Science Ltd. All rights reserved.
PII: S0032-3861(02)00877-7

using nanotube reactors for the control of chain structure and material morphology. Moreover, in co-oligomerization of ethylene and propylene, MAO-grafted MCM-41, generated by in situ hydrolysis of TMA in MCM-41 nanotube pores, was used for supporting $[C_2H_4(1\text{-Ind})_2]Zr(CH_3)_2$ catalysts [26]. The polymerization results showed that the MCM-41-supported catalysts were even more active than the corresponding silica-supported or homogeneous systems and the polymer molecular weight increased with the decrease of MCM-41 pore size [26]. Studies on isotactic polypropylene with MCM-41-supported rac-$Et(Ind)_2ZrCl_2$ [22] and syndiotactic polypropylene with MCM-41-supported $[Me_2C(Cp)(Flu)]ZrCl_2$ [32] also showed that the resulted polymers had higher stereoregularity and melting point than homogeneous or silica-supported systems. The polymerization behaviors were also very different. More recently, ethylene copolymerizations with α-olefins was conducted using $Et(Ind)_2ZrCl_2$ catalysts supported on MCM-41, showing significant effects of the nanotube structure on comonomer incorporation and polymerization behavior [23].

There are numerous studies on the Ni-diimine catalysts impregnated on inorganic supports [33–38], such as silica, clay, and polymeric supports [39]. However, nanotube particle-supported Ni-diimine catalysts have not been reported. The unique characteristic of the controllable nanotube diameter and particle morphology may provide a good model system to study the effects of support morphology on catalyst impregnation and polymerization. The nanotube structure may influence the Ni-diimine catalyst performance, such as chain walking, during polymerization.

In this work, we used the particles with different morphological parameters as support for a Ni-diimine catalyst (DMN, 1,4-bis(2,6-diisopropylphenyl) acenaphthene diimine nickel(II) dibromide). The supported catalysts were used for slurry polymerization of ethylene. The objectives of this experimental work are to evaluate the effects of such parameters as pore diameter and particle size on the catalyst impregnation, and to elucidate the effects of nanotube geometric constraints on chain walking process, polymer structure and polymerization behavior.

2. Experimental

2.1. Materials

All manipulations involving air and/or water sensitive compounds were performed in dry nitrogen glove box or under nitrogen protection. The α-diimine ligand (ArN=C(An)–C(An)=NAr, An = acenaphthene, Ar = 2,6-(*i*-$Pr)_2C_6H_3$) and the dibromide nickel-diimine catalyst (DMN, (ArN=C(An)–C(An)=NAr)$NiBr_2$) were synthesized following the procedures reported in literatures [3]. Modified methylaluminoxane aluminum (MMAO-3A) was provided by Akzo-Nobel Corporation, as 7.25 wt% aluminum in toluene. Polymerization-grade ethylene (from Matheson Gas) was purified by passing it through CuO, Ascarite, and 5A molecular sieves. Toluene (anhydrous grade, from Aldrich) was refluxed over sodium with benzophenone as indicator and distilled under nitrogen atmosphere prior to use.

2.2. Synthesis and characterization of MCM-41 and MSF particles

Three MCM-41 particles with different pore sizes and particle sizes and one MSF particle were synthesized and used as supports for this work. These particles were all silicate-based and were synthesized according to the literature procedures. [19,40–42]. The particles were all calcinated in air at 550 °C for 6 h for the removal of surfactants.

X-ray diffraction (XRD) and nitrogen adsorption-desorption isotherm were used to characterize internal structure of the calcinated particles. The X-ray powder diffraction spectra were recorded on a Bruker D8 Advance diffractometer. Nitrogen adsorption-desorption isotherms were measured at 77 K using an ASAP2010 volumetric adsorption apparatus from Micrometritics. Prior to the analysis, the samples were degassed under vacuum at 200 °C for 2 h. The specific surface areas of the samples were obtained based on the standard BET method. The average pore diameter was calculated using BJH method. An Electroscan ESEM 2020 was used for investigating the particle morphology.

2.3. Preparation of particle-supported catalysts

Two supporting methods were used in this work for the impregnation of DMN on the nanotube particles. Method (a): 1.0 g of calcinated particles was heated at 200 °C under vacuum for 8 h. It was then directly mixed with 60 ml toluene solution of 0.6 mmol DMN. After stirring for 12 h at room temperature, the slurry was filtered; the solid was collected and washed seven times with 70 ml toluene and once with 70 ml anhydrous pentane. The supported catalyst was then dried under vacuum at room temperature for overnight. Method (b): 1.0 g of calcinated particles was heated at 200 °C under vacuum for 8 h. It was then mixed with 50 ml toluene solution of 6 mmol Al of MMAO. The slurry was stirred overnight at room temperature. The solid was filtered, washed five times with 100 ml of toluene and once with 70 ml of pentane, and then dried under vacuum at room temperature. Subsequently, the MMAO-pretreated particle was mixed with 60 ml toluene solution of 0.6 mmol DMN. After stirring for 12 h at room temperature, the solid was collected by filtration, washed seven times with 70 ml of toluene and once with 70 ml pentane, and then dried overnight under vacuum at room temperature.

The ICP-MS analysis was used to determine the supported Al and Ni amounts on the particles. About

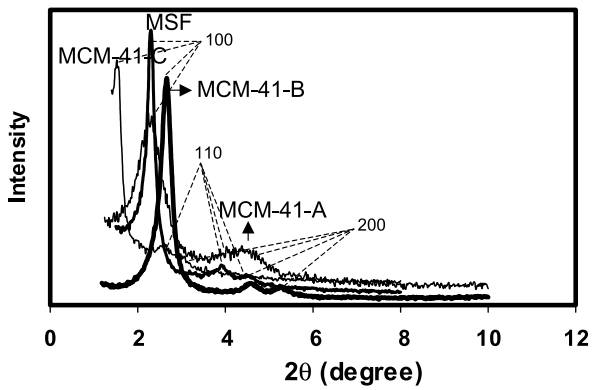

Fig. 1. XRD spectra of the mesoporous particle samples used in this work as catalyst supports.

10 mg of the supported catalysts was dissolved with HF and HNO_3 acid on a hotplate. After a complete dissolution, the solution was diluted with distilled water and used for the ICP-MS analysis.

2.4. Polymerization

The high-pressure ethylene slurry polymerizations with homogeneous or supported DMN catalysts were conducted in a 1-liter autoclave stainless steel reactor. The reactor was carefully cleaned with acetone, heated to 140 °C under vacuum for 2 h, purged five times with UHP nitrogen, and then cooled down to room temperature. 400 ml toluene and required amount of MMAO solution were added into the reactor under nitrogen protection. The mixture was stirred for 10 min while being heated up to the reaction temperature. The catalyst solution or suspension was then injected into the reactor; the system was stirred for 10 min and then pressurized to the desired ethylene pressure to start the polymerization. The reactor temperature was controlled at a set temperature within ±0.5 °C by water/ethylene glycol cool circulator. The reaction was stopped by venting the reactor and adding 20 ml of acetone. The polymer produced was filtered, washed with a large amount of methanol and then dried under vacuum at 50 °C overnight.

Polymerization with homogeneous DMN catalyst at 1 atm ethylene pressure was conducted in a 500 ml glass flask. 200 ml of toluene was added to the flame-dried flask under 1 atm of ethylene pressure at the set temperature maintained by an oil bath. Then a desired amount of MMAO (Al/Ni (mol) = 2000) solution was added under stirring. The polymerization was started by injecting the catalyst solution, and was terminated by venting the system and adding 20 ml of acetone. The polymer was precipitated, washed with methanol, and dried overnight at 50 °C under vacuum.

2.5. Polymer characterization

The DSC analysis was conducted using Thermal Analysis 2910 MDSC from TA Instruments in the standard DSC mode. UHP N_2 gas at a flow rate of 30 ml/min was purged through the calorimeter. A refrigerated cooling system (RCS) with the cooling capacity to 220 K was attached to the DSC cell. The temperature and heat capacity for the instrument were initially calibrated with indium standard at the heating rate of 10 °C/min. The polymer sample (about 5 mg) was first heated to 180 °C at the rate of 10 °C/min to remove thermal history. It was then cooled down to 0 °C at 5 °C/min. A second heating cycle was used for the acquisition of the DSC thermogram at the scanning rate of 10 °C/min. Polymer molecular weight (MW) and molecular weight distribution (MWD) were measured at 135 °C in 1,2,4-trichlorobenzene using Waters Alliance GPCV 2000 with DRI detector coupled with an in-line capillary viscometer. The polymer molecular weight was calculated according to a universal calibration curve based on polystyrene standards. 75.4 MHz ^{13}C NMR analysis was conducted on a Bruker AV300 pulsed NMR spectrometer with Waltz-supercycle proton decoupling at 120 °C. The polymer sample was dissolved in 1,2,4-trichlorobenzene and deuterated *o*-dichlorobenzene mixture in 10 mm NMR tubes with concentration about 20 wt%. At least 4000 scans were applied for each acquisition to obtain a good signal-to-noise ratio. SEM study on polymer morphology was carried out on Electroscan ESEM 2020 facility. EDX-TEM study on microtomed polymer samples was carried out on JEOL 1200EX facility.

3. Results and discussion

3.1. Characterization of the nanotube particles

Three MCM-41 particles (MCM-41-A, MCM-41-B,

Table 1
Structural parameters for the mesoporous materials

Support	S_{BET} (m^2/g)	d_p (Å)	V_p (ml/g)	d_{100} (Å)	a (Å)	b (Å)	L_c (μm)	Preparation method
MCM-41-A	743.5	22.7	0.63	38.9	44.9	22.2	30	Ref. 40
MCM-41-B	1231.6	21.4	1.01	33.3	38.5	16.8	1	Ref. 41
MCM-41-C	829.0	45.1	0.95	55.9	64.5	19.4	15	Ref. 42
MSF	952.3	27.0	0.80	38.4	44.3	17.3	350	Ref. 19

S_{BET}, BET specific pore surface area; d_p, average pore diameter, obtained from BJH adsorption data; V_p, volume of pores; d_{100}, XRD interplanar spacing; a, distance between neighboring pore centers, $a = 2d_{100}/3^{1/2}$; b, pore wall thickness, $b = a - d_p$; L_c, characteristic nanotube length from SEM.

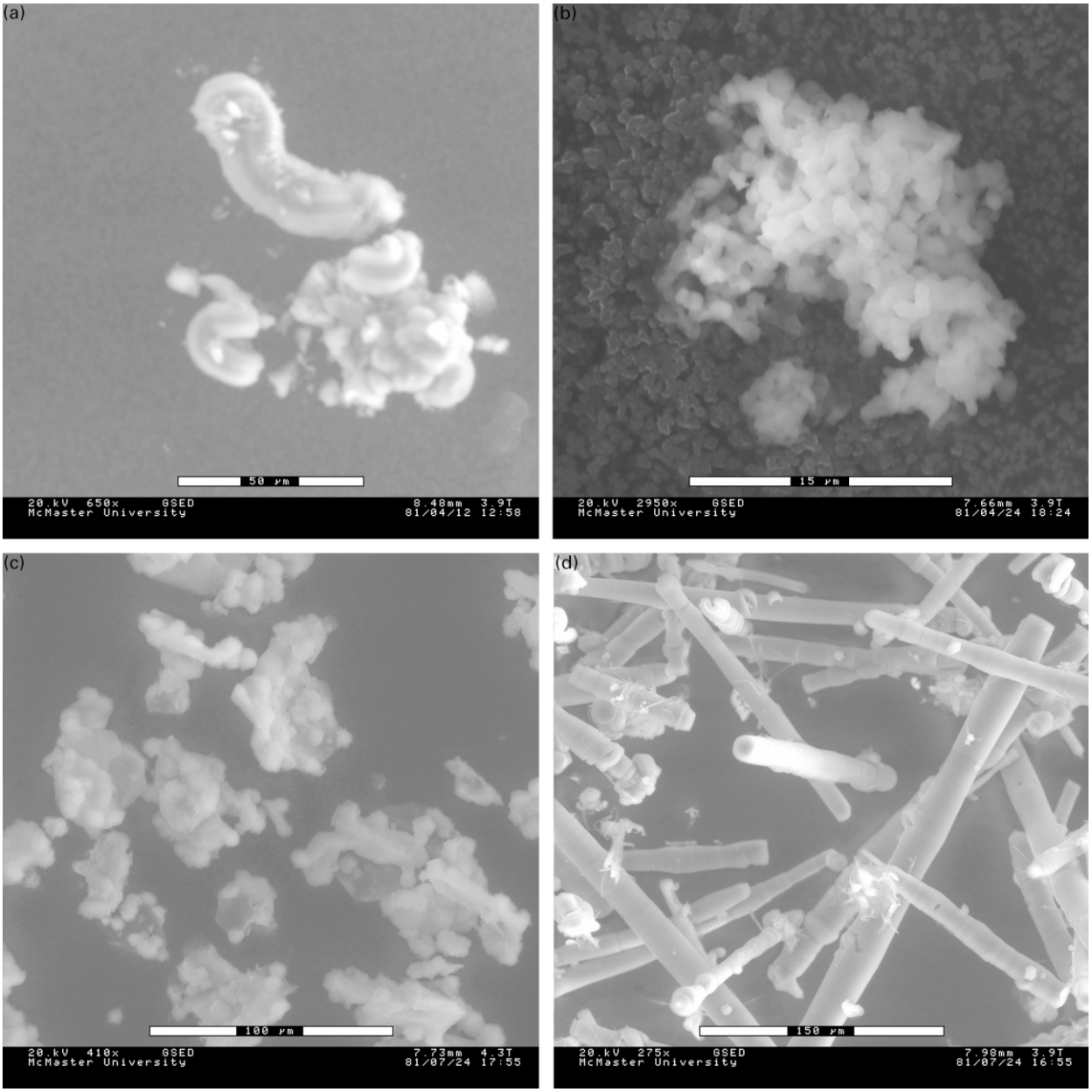

Fig. 2. SEM photographs of the mesoporous particles: (a) MCM-41-A (scale bar: 50 μm); (b) MCM-41-B (scale bar: 15 μm); (c) MCM-41-C (scale bar: 100 μm); (d) MSF (scale bar: 150 μm).

MCM-41-C) and one MSF particle, different in nanopore size, particle size and morphology, were used as supports for the DMN catalyst in this work. Fig. 1 shows the XRD spectra for the calcinated particles. Table 1 summarizes the particle morphological parameters, including specific surface area, average pore diameter, pore volume, and pore wall thickness, from the nitrogen adsorption–desorption and XRD analyses. All the particles have very high specific surface area ($>700\ m^2/g$), high pore volume (0.63–1.01 ml/g) and nano-range average pore diameter (2.1–4.5 nm). MCM-41-A, MCM-41-B and MSF have similar average pore diameters. However, the pore size of MCM-41-C is much bigger. All the particles have similar pore wall thickness. The XRD spectra show that these particles have quite uniform long-range ordered hexagonal nanotube structures. In addition to the main [100] diffraction, the higher order [110] and [200] diffractions are observable. Compared to the other three particles, MCM-41-A has a broader distribution of [100] diffraction, showing a broader pore size distribution.

The particles are also distinctively different from each other in particle size and morphology. Fig. 2 shows their SEM photographs. MCM-41-A has curved tubular structure of about 10–50 μm in length (equivalent to nanotube length) and about 10 μm in diameter (each particle consists of thousands to millions nanotubes). MCM-41-B particles

Table 2
Effect of supporting method on the impregnation of DMN catalysts to MCM-41-B

Catalyst system	Catalyst	Support	Ni or Ti load[a]	Al load[a]	Support method	Catalyst activity[b]
MCM-Ni-a	DMN	MCM-41-B	0.0184	–	a	41
MCM-Ni-b	DMN	MCM-41-B	0.217	2.71	b	8.0×10^3
MCM-Ti-a	Cp_2TiCl_2	MCM-41-B	0.143	–	a	–

[a] Loaded amounts of Ni or Ti and Al are in mmol of metal per gram of the supported catalyst system (including catalyst and support).
[b] Catalyst activity is in kg PE produced per mol-Ni per hour. The polymerization conditions are: ethylene pressure: 200 psig; reaction temperature: 35 °C; reaction time: 1 h; amount of supported catalyst system (including catalyst and support): MCM-Ni-a 0.11 g, MCM-Ni-b 0.017 g, equivalent to the Ni contents of 2.0 μmol and 3.7 μmol, respectively; in 400 ml toluene; Al/Ni ratio: 2000 (molar).

are loose agglomerates of about 15 μm consisting of many small tubular particles of about 1 μm diameter. Like MCM-41-B, MCM-41-C is also agglomerates of particles with sizes of about 15 μm. MSF has long-range highly ordered fiber structure with fiber lengths about 150–500 μm and fiber diameters in the range of 10–30 μm. The characteristic tube lengths for these materials are also summarized in Table 1. These long-range ordered fibers were demonstrated for applications as waveguide and laser materials [19,20]. A recent study on the internal structure of MSF showed that nanotubes inside the fiber were wound in a helical manner along the fiber axial direction [21]. On the other side, the MCM-41 nanotubes run parallel to the axis.

3.2. Effect of supporting method on DMN catalyst impregnation

The supporting method has a significant effect on catalyst immobilization and characteristics of supported catalysts. There are three major supporting methods applicable for the immobilization of metallocene and other homogeneous catalysts [13–16]. They are: (a) direct impregnation of catalysts to support, (b) pretreatment of support with MAO or alkylaluminium followed by reaction with catalyst, and (c) immobilization of catalyst ligand on support followed by an addition of transitional metal salt. Different methods give supported catalysts different features due to different steric interaction between catalyst molecules and support surface. The effects of supporting methods on metallocene catalyst properties have been reviewed by Ribeiro et al [13]. However, the effect of supporting method on Ni-diimine catalyst impregnation has not yet been reported.

In this work, Methods (a) and (b) were employed and compared for the impregnation of DMN onto MCM-41-B. In MCM-Ni-a, DMN was directly impregnated on MCM-41-B. In MCM-Ni-b, MCM-41-B was pretreated with MMAO prior to the DMN impregnation. For comparison purposes, a metallocene catalyst, Cp_2TiCl_2, was also supported onto MCM-41-B by Method (a). Table 2 reports the ICP-MS results of for the supported catalysts. A much higher level (over ten times) of loaded DMN catalyst was obtained with Method (b) than with (a). Compared to Cp_2TiCl_2, the catalyst loading for MCM-Ni-a was also much lower.

The significant differences in the loaded amount are attributed to the different reactivity of DMN with the support surface. In Method (a), the supporting mechanism is believed to be through the reaction of DMN with residual hydroxyl groups on the dehydroxylated silica support surface. For metallocene catalysts, studies have shown that, in Method (a), metallocene reacts with hydroxyl on silica surface to form $\equiv Si-OMClCp_2$, which is converted to a catalytic species upon reacting with MAO. It has also been shown that the supported metallocene reactivity changes with metal center type in the order of $Cp_2HfCl_2 > Cp_2ZrCl_2 > Cp_2TiCl_2$ [43]. The result of this work suggests that DMN has lower reactivity with hydroxyl on silica surface than Cp_2TiCl_2. For the MAO-mediated support system in Method (b), it was proposed that MAO molecules were chemically bonded to surface by reacting with hydroxyl groups [44,45]. This MAO-coated surface has a stronger Lewis acidity than the dehydroxylated surface and thus is more reactive toward DMN, resulting in the higher catalyst-loading amount on the support.

The supporting method not only affected the loading, but also changed the characteristics of catalytic active centers. Ethylene polymerizations at 35 °C and ethylene pressure of 200 psig were conducted with both MCM-Ni-a and MCM-Ni-b catalysts. Significant differences in the catalyst activities were observed (see Table 2). MCM-Ni-a had a very low activity, accounting only 0.5% of that of MCM-Ni-b. This extremely low activity of MCM-Ni-a reflects that the reaction of DMN with hydroxyl groups on support surface yielded active sites with much lower ethylene incorporation ability, possibly due to steric and/or electronic effects exerted by the surface. However, for MCM-Ni-b, the active sites more likely floated over MAO-coated surface with less surface constraints and exhibited more similarity to a homogeneous system, as suggested by Chien et al for zirconocene catalysts supported on MAO-treated silica [46].

3.3. Effect of particle structure on catalyst impregnation

The parallel nanotube structure with uniform and controllable pore size makes the particle an excellent model system to study the effects of particle structure, such as nanotube diameter and length, on catalyst impregnation. In this work, the DMN catalyst was impregnated onto the

Table 3
Effect of particle structure on the impregnation of DMN catalysts with Method (b)

Catalyst system	Support	Ni load[a]	Al load[b]	Al/Ni molar ratio[c]
MCM-Ni-1	MCM-41-A	0.156 ± 0.010	1.76 ± 0.23	11.3
MCM-Ni-2	MCM-41-B	0.200 ± 0.020	2.55 ± 0.16	12.8
MCM-Ni-3	MCM-41-C	0.165 ± 0.012	4.56 ± 0.17	27.6
MSF-Ni	MSF	0.0643 ± 0.014	2.93 ± 0.14	45.6

Two impregnation runs were repeated for each support.
[a] Loaded Ni amount in [mmol/(g supported catalyst system)].
[b] Loaded Al amount in [mmol/(g supported catalyst system)]. The supported catalyst system includes supported catalyst and the MMAO-treated support.
[c] Calculated based on the average Ni and Al loads.

four mesoporous supports with Method (b). Table 3 compares the ICP-MS data of the Ni and Al loading amounts for these supported catalysts. The result shows a strong dependence of the catalyst and MMAO impregnation on the support structure. A significantly higher amount of MMAO loading was observed with the MCM-41-C. The MMAO loading increased in the order of MCM-41-A < MCM-41-B < MSF < MCM-41-C. However, a much lower DMN loading was found with MSF. The DMN loading increased in the order of MSF < MCM-41-A < MCM-41-C < MCM-41-B.

The different loading amounts of MMAO and DMN in the four supports can be related to diffusion limitations during the catalyst impregnation that is a molecular diffusion process inside the nanotubes. Different tube diameters and lengths yield different levels of diffusion resistance. Larger diameter and shorter length favor diffusion and thus, favor the impregnation of MMAO and DMN. The nanotube channels of the MCM-41 and MSF particles are one-dimensional. The impregnation process of the MMAO and DMN molecules in these channels can be considered as diffusion into a planar substrate with the channel length (i.e., particle size for MCM-41 and fiber length for MSF) as the characteristic length L_c. The diffusion resistance is inversely proportional to D/L_c, where D is an effective molecular diffusivity [47]. For a molecule of diameter d_m inside a mesopore of diameter d_p in liquid, D is related to the ratio $\lambda = d_m/d_p$ and the molecular diffusivity in bulk liquid D_m such as $D/D_m = \exp(-4.6\lambda)$ [47].

Based on the reported crystallographic studies on the molecular structures of some Ni-diimine complexes [5,48], we estimate the molecular diameter of DMN about 1 nm. The effective diffusivity for DMN in the nanotube can be calculated by $D/D_m = \exp(-4.6\lambda)$ [47]. MMAO has a more complicated oligomeric structure. Studies on the structure of MAO, $[-Al(Me)-O-]_n$, suggested that the MAO molecules could be one-dimensional linear chains or cyclic ring three-dimensional cage structure with $n \approx 5-20$ [49]. Based on the work by Sano and co-workers on the adsorptive separation of MAO by MCM-41 [50], we estimate the molecular diameter of MMAO approximately 2 nm. For the molecules having sizes in this range, their effective diffusivities in mesopores are more accurately described by $D/D_m = 0.984((1-\lambda)/\lambda)^{5/2}$ [47].

Table 4 shows the diffusion resistance parameter $(D/D_m)/L_c$ for the MMAO and DMN molecules in the four different supports. This model provides good explanation for the high MMAO loading on MCM-41-C and the low DMN loading on MSF. The diffusion resistance for DMN increases in the order of MCM-41-B < MCM-41-C < MCM-41-A < MSF, which is consistent with the amount of DMN loaded on the supports. However, the order of diffusion resistance for MMAO is MCM-41-C < MCM-41-B < MCM-41-A ~ MSF, which does not fully agree with the MMAO loading, particularly for MSF probably due to the complicated molecular structure and broad molecular size distribution of MMAO.

3.4. Effect of support on ethylene polymerization activity

To evaluate the performance of supported catalysts and

Table 4
Effect of support structure on diffusion parameters of MMAO and DMN

Supports	d_p (nm)	L_c (μm)	MMAO, $d_m = 2$ nm			DMN, $d_m = 1$ nm		
			λ (d_m/d_p)	D/D_m[a]	$(D/D_m)/L_c$ (μm^{-1})	λ (d_m/d_p)	D/D_m[b]	$(D/D_m)/L_c$ (μm^{-1})
MCM-41-A	2.27	30	0.881	0.00660	0.00022	0.441	0.132	0.00440
MCM-41-B	2.14	1	0.935	0.00125	0.00125	0.467	0.117	0.117
MCM-41-C	4.51	15	0.443	1.74	0.116	0.221	0.361	0.024
MSF	2.70	350	0.741	0.0711	0.000203	0.370	0.182	0.00052

[a] Calculated according to $D/D_m = 0.984((1-\lambda)/\lambda)^{5/2}$.
[b] Calculated according to $D/D_m = \exp(-4.6\lambda)$.

Table 5
Ethylene polymerization using homogeneous Ni-diimine catalysts

Run	Catalyst (Ni-μmol)	Pressure (psig)	Temperature (°C)	Time (min)	Activity[a]	Mn (kg/mol)	PDI	Tm (°C)
1	1.6	15	35	30	4.56	155.2	2.0	–
2	2.0	50	35	20	8.25	131.4	3.1	80
3	1.0	100	35	10	14.8	178.2	2.4	85
4	1.1	100	45	30	23.1	123.4	2.4	76
5	2.0	100	55	30	12.5	103.7	2.4	61
6	1.0	200	35	10	29.5	254.8	2.4	111
7	1.0	200	45	10	26.4	166.3	2.6	99
8	1.0	200	55	10	6.48	137.1	2.4	85
9	1.1	400	35	10	59.3	181.8	2.3	121

Al(MMAO)/Ni molar ratio: 3500; solvent: toluene 400 ml.
[a] in 10^3 kgPE/(mol-Ni hr)

to provide a reference to show the effect of support on the polymerization behavior and polymer chain structure, ethylene polymerizations using homogeneous DMN catalysts were conducted under various reaction conditions. Table 5 shows the polymerization results and polymer properties. The catalyst activity at low ethylene pressure was comparable to the literature data; however, it was lower at high pressure [5]. The melting points were very close to those reported in the literature [5]. With the increase of ethylene pressure and decrease of reaction temperature, the melting point tended to increase, exhibiting a trend of the reduction of short chain branches due to the competition between chain walking and chain propagation processes. There was no clear trend in the change of polyethylene molecular weight with ethylene pressure. Increase in temperature decreased the catalyst activity due to deactivation as reported by Brookhart et al [5]. The polymer molecular weight also decreased at high temperature, due to higher chain transfer rates.

Table 6 presents the ethylene polymerization results with DMN supported on the nanotube particles. Compared to the homogeneous catalyst counterparts, significant reductions in the catalyst activity were observed for all the supported systems under the same reaction conditions. The activity for

Table 6
Ethylene polymerization using supported catalysts

Run	Catalyst and charge	P (psig)	T (°C)	T (min)	Activity[a]	M_n (kg/mol)	PDI	T_m (°C)
1	MCM-Ni-1, 31.3 mg	50	35	30	2.04	133.7	3.1	82, 118
2		100	35	30	3.66	162.0	2.9	99
3		100	55	30	2.19	96.9	3.2	63, 128
4		200	35	60	5.34	179.9	2.8	111, 117
5		200	55	30	2.19	140.9	2.5	82, 116
6		400	35	30	5.40	320.4	2.8	121
7	MCM-Ni-2, 17 mg	50	35	60	1.74	150.2	2.3	76
8		100	35	60	3.64	182.6	3.0	96
9		100	55	30	3.30	106.9	2.2	64
10		200	35	60	8.00	264.3	2.4	111
11		200	55	30	2.13	132.4	2.3	82
12		400	35	30	7.53	232.1	2.6	121
13	MCM-Ni-3, 31.7 mg	50	35	30	2.32	139.0	3.2	73
14		100	35	30	4.39	175.0	2.6	100
15		100	55	30	1.80	118.3	2.7	62
16		200	35	30	5.67	174.5	4.9	111
17		200	55	30	1.98	131.6	2.9	82
18	MSF-Ni, 0.102 g	50	35	30	1.02	161.2	3.0	85, 113
19		100	35	30	1.98	197.1	3.3	99, 115
20		100	55	30	0.568	108.0	2.5	62, 117
21		200	35	30	3.57	199.8	4.0	110
22		200	55	30	0.744	205.9	5.2	82, 121

Al(MMAO)/Ni molar ratio: 2000; solvent: toluene 400 ml.
[a] in 10^3 kgPE/(mol Ni hr).

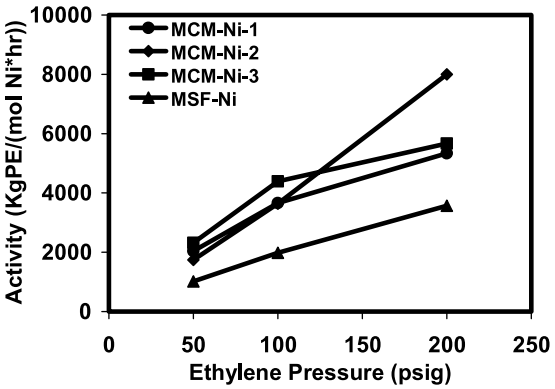

Fig. 3. Ethylene polymerization activity with the mesoporous particle-supported DMN catalysts at 35 °C and different ethylene pressures. Refer to Table 4 for the polymerization conditions.

a supported catalyst system was about 10–30% of that of the corresponding homogeneous system. The significant activity reduction is a common phenomenon for supported catalyst systems and is believed to be due to steric effects exerted by support on catalyst active centers thus limiting the monomer incorporation ability. The activity ratios between the supported and homogeneous systems are very similar to those of metallocene systems. Like the homogeneous system, an increase in temperature lowered the polymerization activity for the supported catalysts due to deactivation.

Fig. 3 shows the polymerization activities for the four supported catalysts at 35 °C and various ethylene pressures. There was no obvious activity difference between the big pore sized MCM-Ni-3 and the small pore sized MCM-Ni-1 and MCM-Ni-2 samples, indicating that the nanopore size had no significant effect on the diffusion limitations of small ethylene molecules inside the nanopores. Surprisingly, a much lower activity, about half of those observed in the MCM-41 supported catalyst systems, was found for the MSF supported catalysts. This significant activity drop is

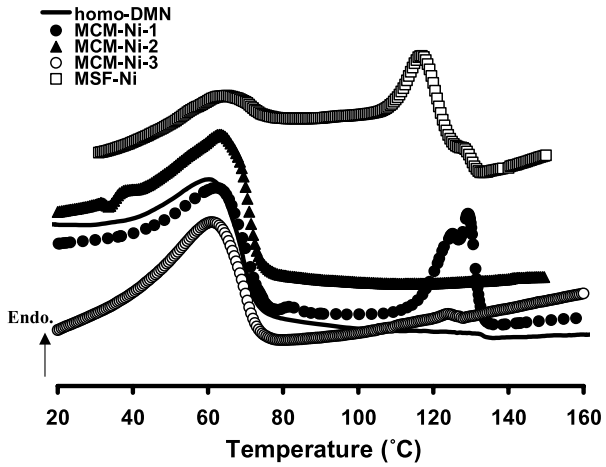

Fig. 4. DSC thermograms for the polymers produced with homogeneous and supported catalysts at ethylene pressure of 100 psig and reaction temperature of 55 °C.

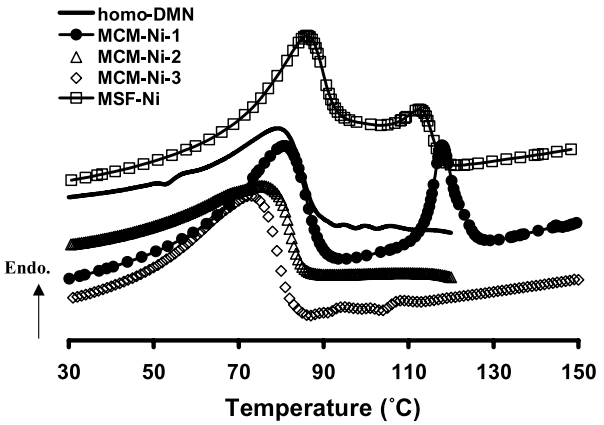

Fig. 5. DSC thermograms for the polymers produced with homogeneous and supported catalysts at ethylene pressure of 50 psig and reaction temperature of 35 °C.

believed to be due to ethylene diffusion limitations in the much longer MSF nanotubes, where the produced polymer chains might block ethylene diffusion. In addition, the much higher Al/Ni ratio in this supported catalyst (Table 3) may influence the catalyst activity and leads to pore blocking by MMAO.

3.5. Effects of support on polymer properties

In a recent patent by Exxon [35] on ethylene polymerization using silica-supported Ni-diimine catalysts, the reduction in polymer molecular weight was observed. However, in this work, as shown in Table 6, there was no clear trend of change in molecular weight compared to the homogeneous systems. However, broadening of the molecular weight distributions was evident with the supported catalyst systems. A PDI of 5.7 was observed in the MSF supported system.

The chain walking mechanism appeared to be present in the supported systems. Similar to the homogeneous catalysts, the melting points of the polymers produced with the supported systems increased with the increase of ethylene pressure and the decrease of reaction temperature through the competition of propagation versus chain walking. However, the melting behaviors were very different. Fig. 4 compares the DSC thermograms of the polyethylene samples prepared at ethylene pressure of 100 psig and temperature of 55 °C. Interestingly, a bimodal melting behavior was observed in the thermograms for the polymers produced with MCM-Ni-1 and MSF-Ni systems. The melting point data are presented in Table 6. The melting temperature is related to the short chain branch density. Increasing short chain branch density decreases lamellar thickness of crystal structure and thus lowers melting temperature.

The bimodal melting behavior shows that the polymer sample was a mixture of two chain populations having different short chain branch densities. In the MCM-Ni-1 polymer, the lower melting temperature region centered at

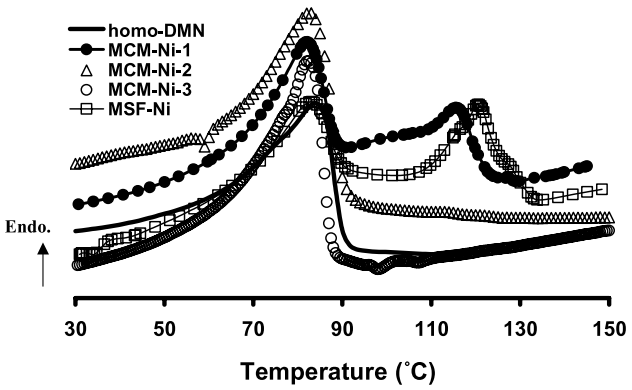

Fig. 6. DSC thermograms of the polymers produced with homogeneous and supported catalysts at ethylene pressure of 200 psig and reaction temperature of 55 °C.

63 °C, being very close to the melting point (61 °C) of the polymers produced with the homogeneous DMN catalyst. These are the chains having high short chain branch densities. The higher melting region centered at 128 °C, corresponding to the chains having much fewer short-chain branches (as a reference, $T_m = 121$ °C for the polymer sample produced with the homogeneous catalyst system at 400 psig and 35 °C). However, the mass fraction of the high Tm chains was small. There were no significant differences in the short chain branch densities among the samples prepared with MCM-Ni-1, MSF-Ni, and homogeneous DMN catalysts. Table 7 presents the short chain branch distributions of the samples.

The bimodal melting behavior was also observed in the polymers produced under some other reaction conditions (see Figs. 5–6) with MCM-Ni-1 and MSF-Ni supported catalysts. A common feature was that the lower melting temperature in the bimodal thermogram was always similar to that of the homogeneous catalyst under the same polymerization conditions. This fraction of chain population was probably generated from the active sites extracted from the support during polymerization. The higher melting temperature was in the range of 113–128 °C and had no clear dependence on the reaction condition. This chain

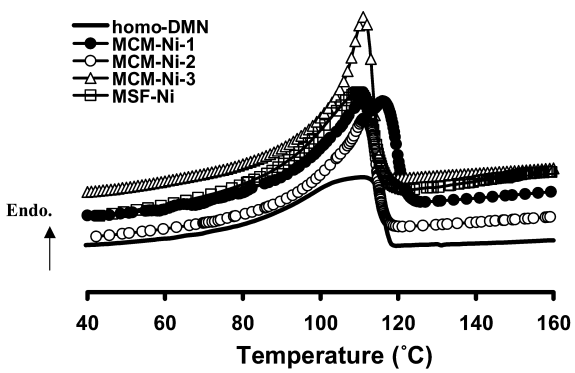

Fig. 7. DSC thermograms of the polymers produced with homogeneous and supported catalysts at ethylene pressure of 200 psig and reaction temperature of 35 °C.

Table 7
Short chain branch densities (per 1000 carbons) for polyethylene produced at 100 psig and 55 °C

Catalyst	Methyl	Ethyl	Propyl	Butyl	Pentyl	Hexyl +	Total
Homo-DMN	45.9	4.9	2.7	2.3	2.1	5.9	63.8
MCM-Ni-1	42.1	4.0	2.7	2.5	2.0	5.0	58.3
MCM-Ni-2	41.7	4.8	3.0	2.7	2.4	5.8	60.4
MCM-Ni-3	41.6	4.8	2.8	2.3	2.2	5.5	59.2
MSF-Ni	45.9	4.5	3.0	2.3	2.1	5.9	63.7

fraction was produced by the unleached active sites. The unleached active sites, due to the strong steric effects exerted by the support, exhibited lower chain-walking rates and therefore produced chains having lower branch density and thus higher melting point. Similar bimodal melting behavior was also observed with other supported systems [37].

The bimodal melting behavior was not observed with the polymer samples prepared by MCM-Ni-2 and MCM-Ni-3 catalysts. These supports had shorter nanotube length and/or bigger pore size, and thus more significant leaching. The polymers produced by these two supported catalysts had similar thermograms as those with homogeneous catalysts, although the ^{13}C NMR analysis (Table 7) showed that these samples had slightly lower short chain branch densities.

Despite the extraction of active sites during polymerization, morphological replication of the supports was observed in the produced polymers. Fig. 8 shows some SEM pictures of the samples prepared at 100 psig and 55 °C. The polymer particles have morphologies resembling their corresponding supports. These particles are totally different from the spherical morphologies produced with an in situ supported DMN/MAO catalyst system reported in the literature [37]. However, there were no individual polymer particles found in all the samples produced in this work. The particles were all agglomerated together. Similar replications were also observed in the polymer samples produced under the conditions of 50 psig/35 °C, 100 psig/35 °C, and 200 psig/55 °C with all the four supported catalyst systems.

In addition to the pore size and particle size, polymerization conditions also affected the chain structure. The bimodal melting behavior was observed for all the polymers with MSF-Ni except for Run 21. The run 21 sample had a very similar thermogram as the homogeneous catalyst (see Fig. 7). A similar observation was made for MCM-Ni-1 in run 6. These results suggest that active site extraction was more complete in these runs. Moreover, the polymer morphology was also very different. Fig. 9 shows a SEM image of the polymer produced in run 21. There is no replication of the support morphology. Similar morphology was found for the polymer produced in run 6. These exceptions may be related to the high polymer productivities due to higher ethylene concentrations at these conditions (200 psig/35 °C, 400 psig/35 °C).

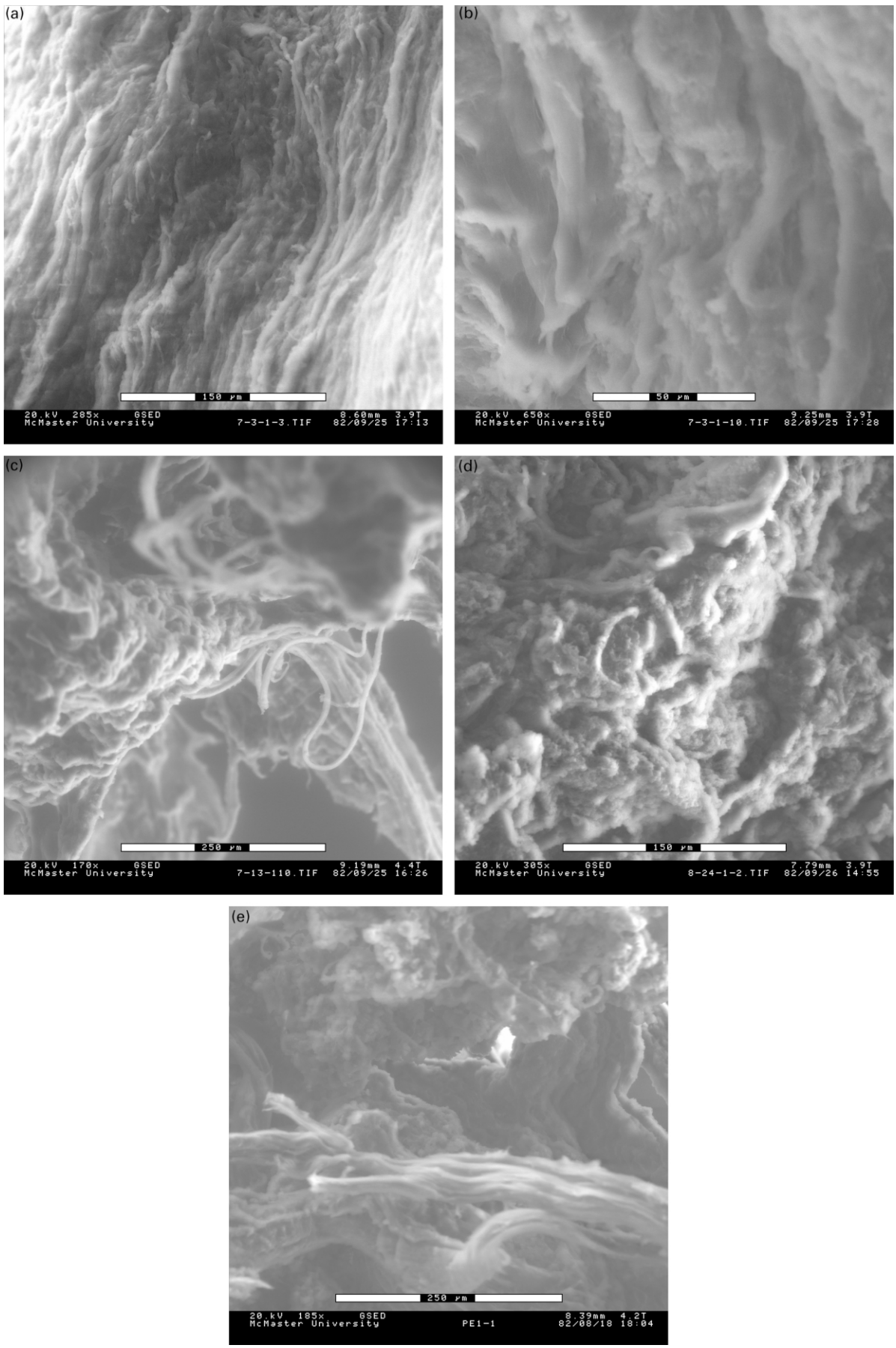
(a)
150 μm
20.kV 285x GSED
McMaster University
8.60mm 3.9T
7-3-1-3.TIF 82/09/25 17:13
(b)
50 μm
20.kV 650x GSED
McMaster University
9.25mm 3.9T
7-3-1-10.TIF 82/09/25 17:28
(c)
250 μm
20.kV 170x GSED
McMaster University
9.19mm 4.4T
7-13-110.TIF 82/09/25 16:26
(d)
150 μm
20.kV 305x GSED
McMaster University
7.79mm 3.9T
8-24-1-2.TIF 82/09/26 14:55
(e)
250 μm
20.kV 185x GSED
McMaster University
8.39mm 4.2T
PE1-1 82/08/18 18:04

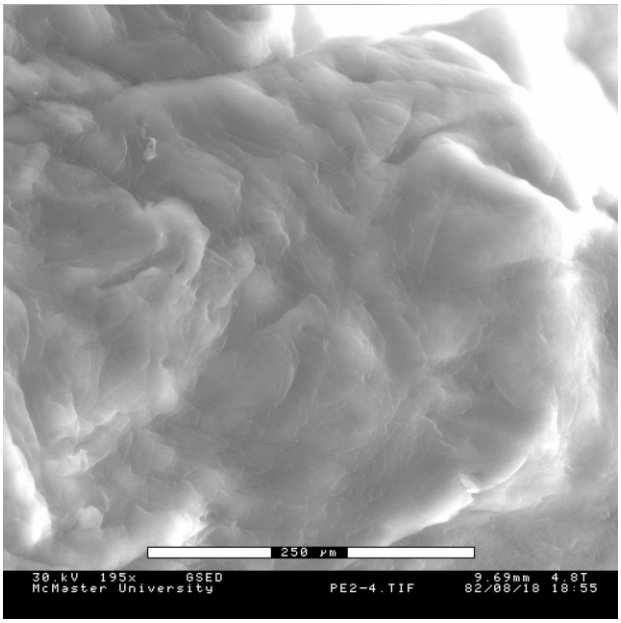

Fig. 9. SEM photograph of the polymer produced in Run 21 with MSF-Ni catalyst (scale bar: 250 μm)

An important phenomenon in olefin polymerization with supported catalysts is the fragmentation of catalyst particle during polymerization due to the hydraulic force caused by fast polymer growth [16]. The degree of fragmentation is related to the support structure and polymer productivity. The higher porosity and thinner pore wall of the support and the higher polymer productivity will make the catalyst readily undergo fragmentation. An EDX-TEM study was conducted on the polymer produced in run 21. Irregular silica fragments with sizes around 1 μm were found widely dispersed in the polymer bulk. Fig. 10 shows one TEM picture of a silica fragment.

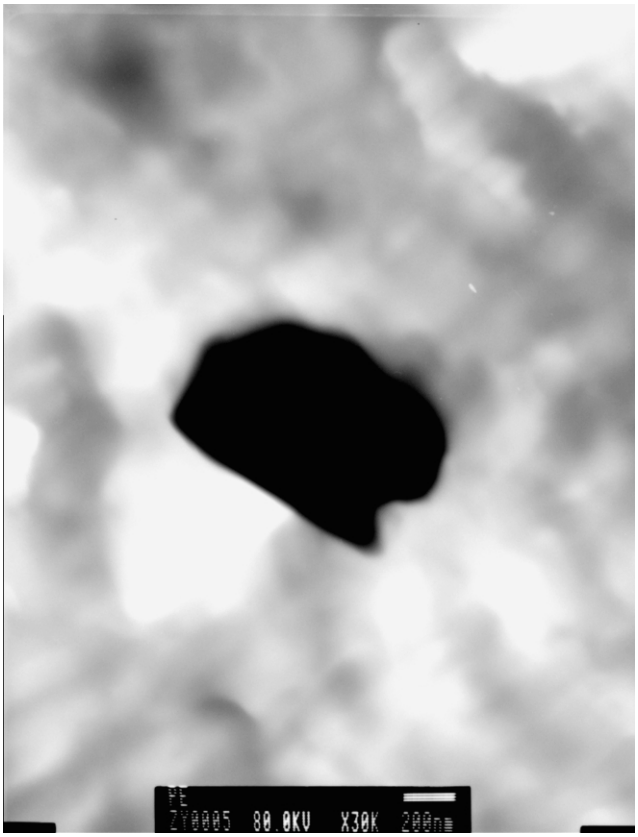

Fig. 10. TEM photograph of the polymer produced in Run 21 with MSF-Ni catalyst (scale bar: 0.2 μm), showing a silica fragment (dark area).

4. Conclusion

Mesoporous particles, including MCM-41 and MSF, with different geometric parameters, such as pore size and particle size, were used as support for a nickel-diimine catalyst (DMN, 1,4-bis(2,6-diisopropylphenyl)acenaphthene diimine nickel(II) dibromide). This study showed that, pretreating the supports with MMAO prior to the DMN impregnation yielded high catalyst loading and high ethylene polymerization activity. The particle parameters strongly affect the catalyst impregnation. Ethylene polymerization was carried out with the particle-supported DMN catalysts. A significant reduction in catalyst activity was observed with the supported systems compared to their homogeneous counterparts. Extraction of the active site from the supports was observed during polymerization. The unleached active sites exhibited much lower chain walking ability and produced polymers with fewer short chain branches. This active site extraction was also related to the mesoporous particle structure and polymerization conditions. Replication of support morphology was found in the polymers produced at some conditions.

Acknowledgements

The authors thank Dr Wen-Jun Wang for his assistance in GPC and ^{13}C NMR analyses of the polymer samples. They also acknowledge Ontario MEST for PREA award, and US

Fig. 8. SEM photographs of the polymers produced at 100 psig and 55 °C: (a) Run 3 with MCM-Ni-1 (scale bar: 150 μm); (b) Higher magnification of (a) (scale bar: 50 μm); (c) Run 9 with MCM-Ni-2 (scale bar: 250 μm); (d) Run 15 with MCM-Ni-3 (scale bar: 150 μm); (e) Run 20 with MSF-Ni catalysts (scale bar: 250 μm).

National Science Foundation (CTS-0080761) for the financial support.

References

[1] Kaminsky W, Arndt M. Adv Polym Sci 1997;127:143.
[2] Ittel SD, Johnson LK, Brookhart M. Chem Rev 2000;100:1169.
[3] Johnson LK, Killian CM, Brookhart M. J Am Chem Soc 1995;117:6414.
[4] Killian CM, Tempel DJ, Johnson LK, Brookhart M. J Am Chem Soc 1996;118:11664.
[5] Gates DP, Svejda SA, Oñate E, Killian CM, Johnson LK, White PS, Brookhart M. Macromolecules 2000;33:2320.
[6] McLain SJ, McCord EF, Johnson LK, Ittel SD, Nelson LTJ, Arthur SD, Halfhill MJ, Teasley MF, Tempel DJ, Killian C, Brookhart MS. Polym Prepr (Am Chem Soc, Div Polym Chem) 1997;38(1):772.
[7] Galland GB, de Souza RF, Mauler RS, Nunes FF. Macromolecules 1999;32:1620.
[8] Jurkiewicz A, Eilerts NW, Hsieh ET. Macromolecules 1999;32:5471.
[9] Guan Z, Cotts PM, McCord EF, McLain SJ. Science 1999;283:2059.
[10] Cotts PM, Guan Z, McCord E, McLain S. Macromolecules 2000;33:6945.
[11] Pappalardo D, Mazzeo M, Pellecchia C. Macromol Rapid Commun 1997;18:1017.
[12] Simon LC, Mauler RS, de Souza RF. J Polym Sci, Part A: Polym Chem 1999;37:4656.
[13] Ribeiro MR, Deffieux A, Portela MF. Ind Eng Chem Res 1997;36:1224.
[14] Abbenhuis HCL. Angew Chem, Int Ed 1999;38:1058.
[15] Hlatky GG. Chem Rev 2000;100:1347.
[16] Fink G, Steinmetz B, Zechlin J, Przybyla C, Tesche B. Chem Rev 2000;100:1377.
[17] Kresge CT, Leonowicz ME, Roth WJ, Vartuli JC, Beck JS. Nature 1992;359:710.
[18] Beck JS, Vartuli JC, Roth WJ, Leonowicz ME, Kresge CT, Schmitt KD, Chu CTW, Olson DH, Sheppard EW, McCullen SB, Higgins JB, Schlenker JL. J Am Chem Soc 1992;114:10834.
[19] Huo Q, Zhao D, Feng J, Weston K, Buratto SK, Stucky GD, Schacht S, Schüth F. Adv Mater 1997;9:974.
[20] Marlow F, McGehee D, Zhao D, Chmelka B, Stucky G. Adv Mater 1999;11:632.
[21] Marlow F, Spliethoff B, Tesche B, Zhao D. Adv Mater 2000;12:961.
[22] Ko YS, Han TK, Park JW, Woo SI. Macromol Rapid Commun 1996;17:749.
[23] Ko YS, Woo SI. Macromol Chem Phys 2001;202:739.
[24] Tudor J, O'Hare D. Chem Commun 1997;603.
[25] O'Brien S, Tudor J, Maschmeyer T, O'Hare D. Chem Commun 1997;1905.
[26] Van Looveren LK, Geysen DF, Vercruysse KA, Wouters BH, Grobet PJ, Jacobs PA. Angew Chem, Int Ed 1998;37:517.
[27] Van Looveren LK, De Vos DE, Vercruysse KA, Geysen DF, Janssen B, Jacobs PA. Catal Lett 1998;56:53.
[28] Rahiala H, Beurroies I, Eklund T, Hakala K, Gougeon R, Trens P, Rosenholm JB. J Catal 1999;188:14.
[29] Kageyama K, Tamazawa J, Aida T. Science 1999;285:2113.
[30] Rao RR, Weckhuysen BM, Schoonheydt RA. Chem Commun 1999;445.
[31] Weckhuysen BM, Rao RR, Pelgrims J, Schoonheydt RA, Bodart P, Debras G, Collart O, Van Der Voort P, Vansant EF. Chem -Eur J 2000;6:2960.
[32] Kaminsky W, Strűbel C, Lechert H, Genske D, Woo SI. Macromol Rapid Commun 2000;21:909.
[33] Sugimura, K., Yorozu, K., Suzuki, Y., Hayashi, T., JP Patent 09278821, April 8, 1996.
[34] Sugimura, K., Yorozu, K., Suzuki, Y., Hayashi, T., JP Patent 09278822, April 8, 1996.
[35] Vaughan, G.A., Canich, JAM, Matsunaga PT, Gindelberger D.E., Squire, K.R., WO Patent Application, 9748736, June 17, 1996.
[36] MacKenzie, P.B., Moody, L.S., Killian, C.M., Lavoie, G.G., WO Patent Application 9962968, Jan 22, 1998.
[37] Simon LC, Patel H, Soares JBP, de Souza RF. Macromol Chem Phys 2001;202:3237.
[38] Preishuber-Pflugl P, Brookhart M. Macromolecules 2002;35:6074.
[39] Bennett, A.M.A., McLain, S.J., WO Patent Application, 9856832, June 9, 1997.
[40] Mokaya R, Zhou W, Jones W. Chem Commun 1999;51.
[41] Cai Q, Lin W-Y, Xiao F-S, Pang W-Q, Chen X-H, Zou B-S. Microporous Mesoporous Mater 1999;32:1.
[42] Sayari A, Liu P, Kruk M, Jaroniec M. Chem Mater 1997;9:2499.
[43] Dufrenne NG, Blitz JP, Meverden CC. Microchem J 1997;55:192.
[44] Soga K, Nakatani H. Macromolecules 1990;23:957.
[45] Soga K, Kaminska M. Makromol Chem Rapid Commun 1992;13:221.
[46] Chien JC, He D. J Polym Sci Part A: Polym Chem 1991;29:1603.
[47] Karger J, Ruthven DM. Diffusion in zeolite and other microporous solids. New York: Wiley; 1992. Chapter 11.
[48] Liimatta JO, Lőfgren B, Miettinen M, Ahlgren M, Haukka M, Pakkanen TT. J Polym Sci Part A: Polym Chem 2001;39:1426.
[49] Chen EYX, Marks TJ. Chem Rev 2000;100:1391.
[50] Sano T, Doi K, Hagimoto H, Wang Z, Toshiya U, Soga K. Chem Commun 1999;733.